Nuclear Materials and Energy 17 (2018) 1–8

Contents lists available at ScienceDirect

Nuclear Materials and Energy

journal homepage: www.elsevier.com/locate/nme

ODS ferritic steels obtained from gas atomized powders through the STARS processing route: Reactive synthesis as an alternative to mechanical alloying

David Pazos[a,b], Arturs Cintins[c], Vanessa de Castro[d], Pilar Fernández[e], Jan Hoffmann[f], Wilfredo García Vargas[g], Teresa Leguey[d], Juris Purans[c], Andris Anspoks[c], Alexei Kuzmin[c], Iñigo Iturriza[a,b], Nerea Ordás[a,b,*]

[a] Ceit-IK4, San Sebastian 20018, Spain
[b] University of Navarra, Tecnun, San Sebastian 20018, Spain
[c] Institute of Solid State Physics, University of Latvia, Riga 1063, Latvia
[d] University Carlos III Madrid, Leganés 28911, Spain
[e] Association EURATOM-CIEMAT, Madrid 28040, Spain
[f] Karlsruhe Institute of Technology, Eggenstein-Leopoldshafen 76344, Germany
[g] TLS Technik GmbH & Co. Spezialpulver KG, Bitterfeld 06733, Germany

A B S T R A C T

Oxide Dispersion Strengthened Ferritic Stainless Steels (ODS FS) are candidate materials for structural components in fusion reactors. Their ultrafine microstructure and the presence of a very stable dispersion of Y-Ti-O nanoclusters provide reasonable fracture toughness, high mechanical and creep strength, and resistance to radiation damage at the operation temperature, up to about 750 °C.

An innovative route to produce ODS FS with composition Fe-14Cr-2W-0.3Ti-0.3Y_2O_3 (wt.%), named STARS (Surface Treatment of gas Atomized powder followed by Reactive Synthesis), is presented. This route avoids the mechanical alloying (MA) of the elemental or prealloyed powders with yttria to dissolve the yttrium in the ferritic matrix.

In this study, starting powders containing Ti and Y are obtained by gas atomization at laboratory and industrial scale. Then, a metastable Cr- and Fe- rich oxide layer is formed on the surface of the powder particles. During consolidation by HIP the metastable oxide layer at Prior Particle Boundaries (PPBs) dissociates, the oxygen diffuses towards saturated solutions or metallic Ti- and Y-rich particles, and Y-Ti-O nano-oxides (mainly Y_2TiO_5) precipitate in the ferritic matrix.

Detailed Microstructural characterization by X-ray Photoelectron Spectroscopy (XPS), X-ray Absorption Spectroscopy (XAS), Scanning Electron Microscopy (SEM) and Transmission Electron Microscopy (TEM) of powders and consolidated materials is presented and correlated with mechanical behaviour.

1. Introduction

Oxide dispersion strengthened ferritic stainless steels (ODS FS) are candidates as structural materials in future fusion and fission reactors. They have demonstrated high stability at elevated temperatures and high creep resistance, and good behaviour under irradiation [1–6]. Their outstanding performance is directly connected to their ultrafine grained microstructure and the presence of highly stable Y-Ti-O nanoparticles, which mitigate irradiation-induced defects like void swelling, phase instabilities or grain boundary embrittlement by helium bubbles [7–9].

The traditional route to produce ODS steels relies on the MA of the elemental or prealloyed Fe-Cr-W-Ti powders with Y_2O_3, Fe-Y or elemental yttrium to dissolve the yttrium in the steel matrix, following by its precipitation as a very fine dispersion of Y-Ti-O nanoclusters during consolidation by hot isostatic pressing (HIP) or hot extrusion [1,2]. This route presents some challenges associated to MA, like long delivery time of powder or contamination from milling media and atmosphere, which have limited the industrial development and commercialization of ODS alloys. Unless special care is taken during MA [10], a contamination due to the wear of WC or high carbon steel milling balls or grinding media is very difficult to avoid, and C level can increase from low levels in the as-atomized powder (50 ppm) up to 320 or even 1700 ppm, depending on the MA conditions [11–14]. Romanoski [15] proposed that typical increase in C content is about 400 ppm per 24 h of MA. Contamination can promote coarse $M_{23}C_6$ or M_3C precipitation, preferentially at grain boundaries, and local partial Cr depletion, which, at the end, result in the degradation of tensile ductility, impact properties and corrosion resistance, unless they are dissolved and re-precipitated by means of suitable thermomechanical treatments (TMTs) [16]. The source of N and O contamination lies in the presence of air inside the vials during MA and, although the O level can be introduced

* Corresponding author.
E-mail address: nordas@ceit.es (N. Ordás).

https://doi.org/10.1016/j.nme.2018.06.014
Received 15 December 2017; Received in revised form 1 May 2018; Accepted 18 June 2018
Available online 09 August 2018

Table 1
Composition of as-atomized powders.

Elem.	Composition wt.%					Contaminants (ppm)			
	Fe	Cr	W	Ti	Y	O	N	C	S
Ceit	Bal.	13.88	1.98	0.30	0.23	250	10	90	20
TLS	Bal.	14.10	1.90	0.27	0.20	216	64	60	5

deliberately to adjust it to the optimum content, the increase in the N content should be limited to lowest possible values, to avoid the precipitation of nitrides or the extension of the γ loop of the Fe-Cr phase diagram to higher contents [17]. However, it is very difficult to avoid N pickup, and N values over 1000 ppm have been reported [12,18]. Only in those cases in which the MA atmosphere can be thoroughly controlled, N concentration reaches lower values (120 ppm) [11,14].

The novelty of the STARS route (Surface Treatments of gas Atomized powder followed by Reactive Synthesis), developed by Ceit to produce ODS alloys, consists in the atomization of metallic powders already containing the ODS phase precursors and, hence, avoids the need for MA to introduce yttrium in the prealloyed powder [19–22]. After atomization in argon, the yttrium of Fe-14Cr-2W-0.3Ti-0.24Y powders is dissolved in the matrix or forms intermetallic compounds. The use of inert gas during atomization minimizes the oxygen gain and, therefore, powder particles need to be oxidized to obtain the required oxygen content to form the Y-Ti-O nanoparticles. During oxidation, a metastable Cr- and Fe- rich and extremely thin oxide layer develops at the surface of powder particles [21], which dissociates during HIP consolidation at elevated temperatures. The oxygen available diffuses inside grain boundaries, reacts with the metallic yttrium and titanium, and Y-Ti-O nanometric particles precipitate. Exhaustive control of the oxidation kinetics of the atomized powder, and understanding of the diffusion and precipitation mechanisms involved in the STARS route is essential to obtain the appropriate distribution of Y-Ti-O nanoparticles. The STARS route is based on the Gas Atomization Reaction Synthesis (GARS) method developed at the AMES Laboratory, in USA to produce ODS microstructures without mechanical alloying, taking advantage of the internal oxidation processes [23,24]. The main difference between the two routes is that, whereas the GARS route atomizes with a reactive gas (Ar + O_2) and, hence, surface oxidation of powders occurs at high temperature, in the STARS route the powder is oxidized at relatively low temperature (below 450 °C), under logarithmic oxidation kinetics [22], to achieve a fine control of the oxygen uptake.

This study presents SEM, TEM and XAFS characterization of ODS FS powders and consolidated materials, obtained from powder atomized at laboratory (Ceit) and industrial scale (TLS Technik GmbH & Co. Spezialpulver KG, henceforth TLS), with different oxidation levels and consolidated at various HIP conditions. The results are correlated with mechanical characterization.

2. Experimental procedure

Powders were produced by VIGA (Vacuum Inert Gas Atomization) at Ceit (2.2 kg) and by EIGA (Electrode Induction Gas Atomization) at TLS (15 kg). The chemical composition (Table 1) of as-atomised powders was analysed by inductively coupled plasma optical emission spectroscopy (ICP-OES), and the results are shown in Table 1. The concentrations of nitrogen and oxygen, and of carbon and sulphur were measured with the inert gas fusion and the combustion infrared detection principles, respectively. The values obtained, shown in Table 1, are significantly lower than those reported after the conventional MA process [11–18].

Atomized powders were sieved into two particle size distributions, < 20 μm and 20–45 μm, and oxidized at temperatures ranging from 175 to 350 °C during 8–12 h. Different sample powders were obtained with their oxygen concentration ranging from 400 to 1500 ppm to study its effect on the density and the nature of the oxide nanoparticles. Oxidized powders were consolidated by HIP at 1220–1300 °C, 120–140 MPa and 1–4 h. Additionally, the combination of HIP consolidation at low temperature, 900 °C, and thermomechanical treatment was explored by hot deformation dilatometry at 900 °C (ε = 1.1), in a Bähr DIL805D deformation dilatometer.

Mechanical properties of consolidated samples were evaluated by microhardness (HV1) indentation and tensile tests (RT-700 °C).

The microstructure of powders and consolidated samples was observed by SEM and TEM. Microchemical analysis of particles was performed by EDS on carbon extraction replicas to avoid matrix effects. Foil thickness was measured by EELS (Electron Energy Loss Spectroscopy) on electropolished TEM disks to obtain nanoparticle number densities.

X-ray absorption spectroscopy measurements were performed at room temperature using the multipole wiggler beam line BL22 – CLÆSS at the ALBA synchrotron radiation facility [13]. X-ray radiation was produced by the storage ring operated in the top-up mode at the energy E = 3.0 GeV and the maximum stored current I = 110 mA. The synchrotron radiation was monochromatized using a pair of Si(111) or Si (311) crystals, and focused onto the sample by toroidal mirror. Collimating and focusing mirrors were responsible for harmonic rejection. X-ray absorption near-edge structure (XANES) and extended x-ray absorption fine structure (EXAFS) at the Ti, Fe and Y K-edges were analysed using conventional methodology [14] and two software packages – EDA [15] and Athena [16]. Theoretical calculations of X-ray absorption spectra were performed using the FEFF8.5 L codes [17].

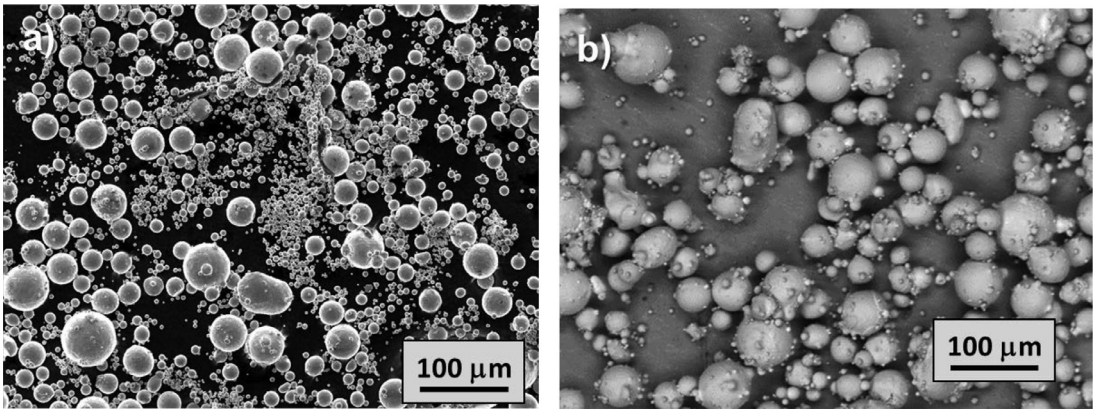

Fig. 1. SEM microstructures showing the morphology of as-atomized (a) Ceit and (b) TLS powders.

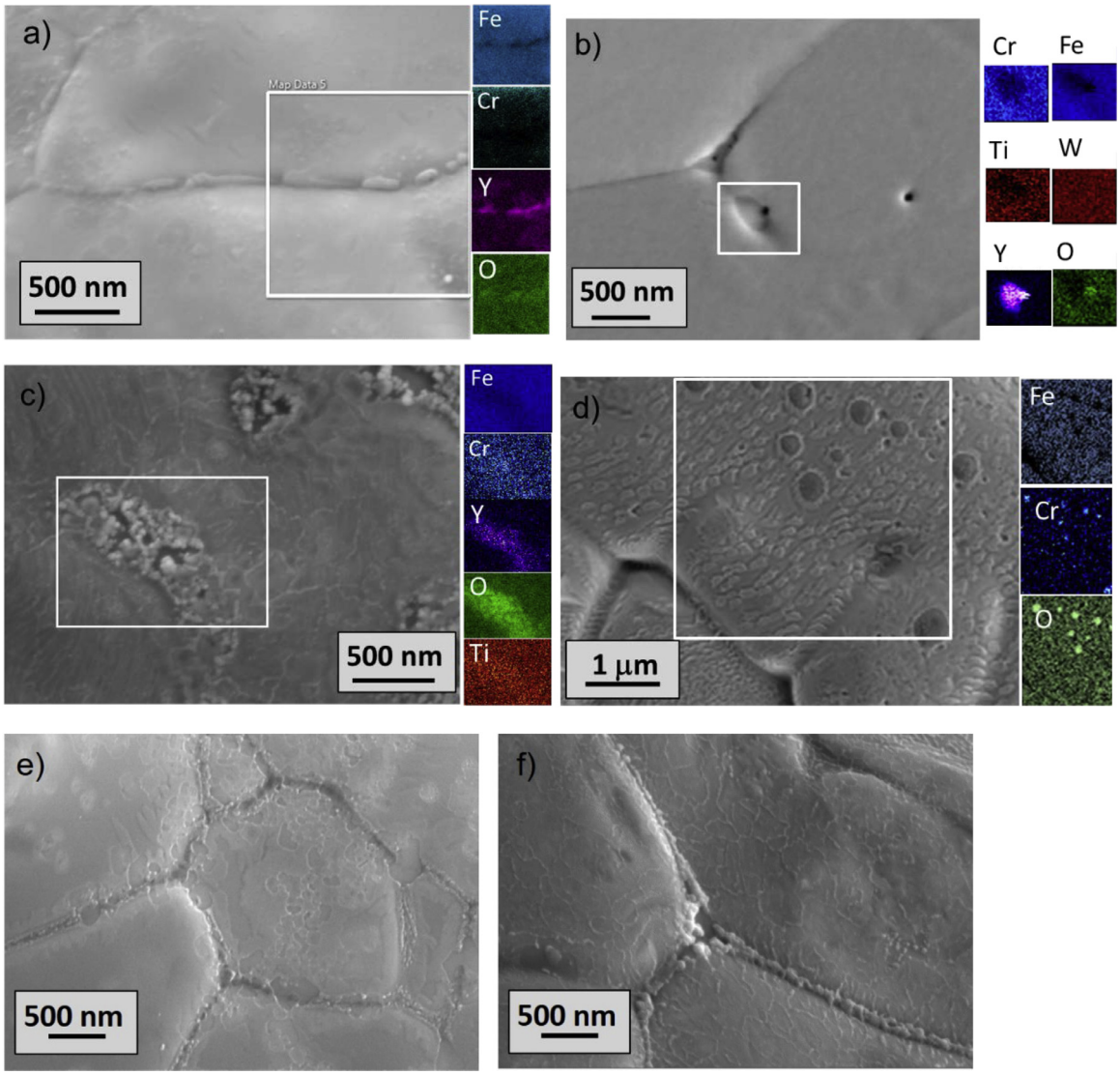

Fig. 2. SEM detailed microstructure of Ceit powders: (a) surface and (b) interior of as-atomized particle, (c), (d) surface of oxidized powder particle and 1500 ppm of oxygen and detail of oxides at surface grain boundaries of powder with (e) 400 ppm and (f) 1500 ppm of oxygen.

3. Results

3.1. Atomization and oxidation of powders

By an appropriate design of the gas atomization procedure and a selection of adequate raw materials, the composition of the atomized powders was close to the target, Fe-14Cr-2W-0.Ti-0.24Y (Table 1). Powder particles are mainly spherical, and in the case of TLS powder, the presence of satellites, caused by collisions between particles during solidification, is very low (Fig. 1).

SEM examination of powder particles at high magnifications and XAS analysis [22] confirmed that yttrium remains metallic and precipitated at grain boundaries, although at the surface it was slightly oxidized, forming almost continuous chains (Fig. 2a and b).

After powder oxidation, Cr_2O_3 chains grow, flanking the prior yttrium-rich chains, which now are also slightly oxidized. In addition, a nanometric continuous Fe_2O_3 layer and discrete Cr_2O_3 particles developed inside grain boundaries (GBs) and the surface of powder particles [12], (Fig. 2c–f). As can be seen in Fig. 2e and f, the thickness of the oxide chains developed at surface grain boundaries grows with increasing oxygen content, and so does the presence of metastable oxides. The maximum thickness of the oxide layer, measured by XPS on powders with highest oxygen content (1500 ppm), was about 20 nm, lower than the oxide thickness measured by Rieken (50–100 nm) by TEM and AES (Auger Electron Spectroscopy) depth profiling [23]. He found that the outer layer was Cr- (and Y-rich) oxide, whereas the inner oxide layer was rich in Cr and Fe.

3.2. Consolidation by HIP at high temperature

HIP consolidation at high temperatures (1220–1300 °C) led to dense materials. SEM microstructural analysis confirmed that finer microstructures are obtained with finer powders (< 20 µm). Higher oxidation degree of powders also promotes grain size refinement (Fig. 3), due to the higher density of oxide NPs, as shown later. Metastable oxides at PPBs dissociated almost completely during HIP, and only

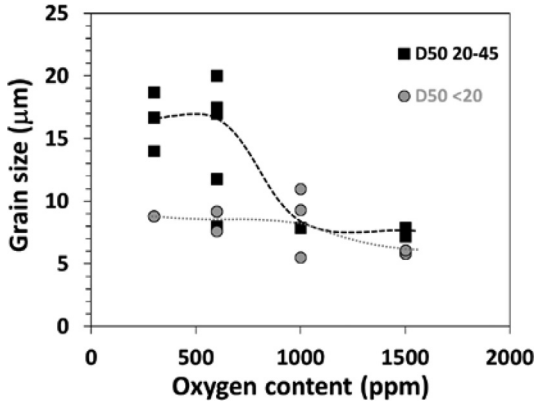

Fig. 3. Evolution of grain size distribution D50 after HIP with oxygen concentration for different powder particles (< 20 μm and 20–45 μm). D50: value of particle diameter at 50% in the cumulative distribution.

submicrometric and nanometric precipitates were observed at grain boundaries (Fig. 4). EDS analysis suggests the presence of two types of precipitates. Ti- and W-rich submicrometric precipitates (bright particles in Fig. 4a, b and d), tentatively identified as $(Ti_{0.9}W_{0.1})C$, are only present in samples with low oxidation degree (< 1000 ppm), or after consolidation at highest temperatures and/or longest times (i.e. 1300 °C 2 h or 1220 °C 4 h). Largest Y-rich oxides (dark 100–200 nm particles in Fig. 4) are located at PPBs and grain boundaries, whereas finest Y-rich oxides (< 50 nm) were observed inside grains.

Y-rich nanoparticles (NPs) are heterogeneously distributed in the ferritic matrix (Fig. 5a–c), regardless of oxygen content, or HIP parameters: some grains contain a high density of NPs below 50 nm ($1 \cdot 10^{22}$ m^{-3}), but others are apparently depleted or their density is lower ($1 \cdot 10^{20}$ m^{-3}). These values are similar to those obtained with the GARS route to produce ODS FS with similar composition to the present work. Rieken [23] estimated by TEM number densities between $1 \cdot 10^{20}$ m^{-3} and $4 \cdot 10^{22}$ m^{-3} for NPs below 60 nm. These values are lower than those observed in ODS FS with similar composition, obtained with the conventional route: [1,6,12,25] and [26] obtained number densities of NPs ranging $1–7 \cdot 10^{23}$ m^{-3} with a diameter of 1–4 nm. In general, 50–60% and 80–90% of the finest NPs (< 50 nm) obtained with the STARS route were smaller than 10 and 20 nm, respectively. The size distribution of NPs is bimodal, with two main peaks at approximately 5–15 nm and 100–150 nm (Fig. 5d). The largest Y-rich NPs, located at PPBs (Fig. 5a, b), were formed during the oxidation of the yttrium that had precipitated at the surface grain boundaries during cooling of atomized powder particles. Their size and density increases with oxidation degree of powder, as well as with powder particle size. The finest NPs are found inside grains, being more abundant in the vicinities of GBs (Fig. 5b). The finest Y-rich NPS inside grains precipitated during consolidation at high temperature: the metastable Cr- and Fe-rich oxides at PPBs dissociate and their oxygen diffuses inside theferritic grains, where it is consumed by metallic yttrium precipitated at GBS (Fig. 2b) or in supersaturated solid solution.

High-resolution transmission electron microscopy (HRTEM) on thin foils (Fig. 5e) and EDS analysis of carbon extraction replicas confirmed that a large fraction of the finest NPs are Y-rich oxides, identified as Y_2O_3, although some of them contain minor presence of Ti (Fig. 5f), and could be identified as Y-Ti-O pyrochlores. EDS (SEM and TEM) analyses suggest that Ti concentration in Y-rich oxide finest NPs increases with oxygen content. For example, the average atomic Ti/Y ratio of Y-Ti-O NPs measured on carbon extraction replicas of Ceit powder (20–45 μm) consolidated at 1220 °C during 4 h increases from 0.03 ± 0.02 to 0.13 ± 0.07 when the oxygen content raises from 300 to 600 ppm. These values are significantly lower than the expected ratios for the $Ti_2Y_2O_7$ and TiY_2O_5 stoichiometric oxides (1 and 0.5 respectively), usually found in Fe-14Cr-2W-0.3Ti-0.3Y_2O_3 ODS FS, and indicate that an important fraction of Ti remains non-oxidized and precipitated as Ti-

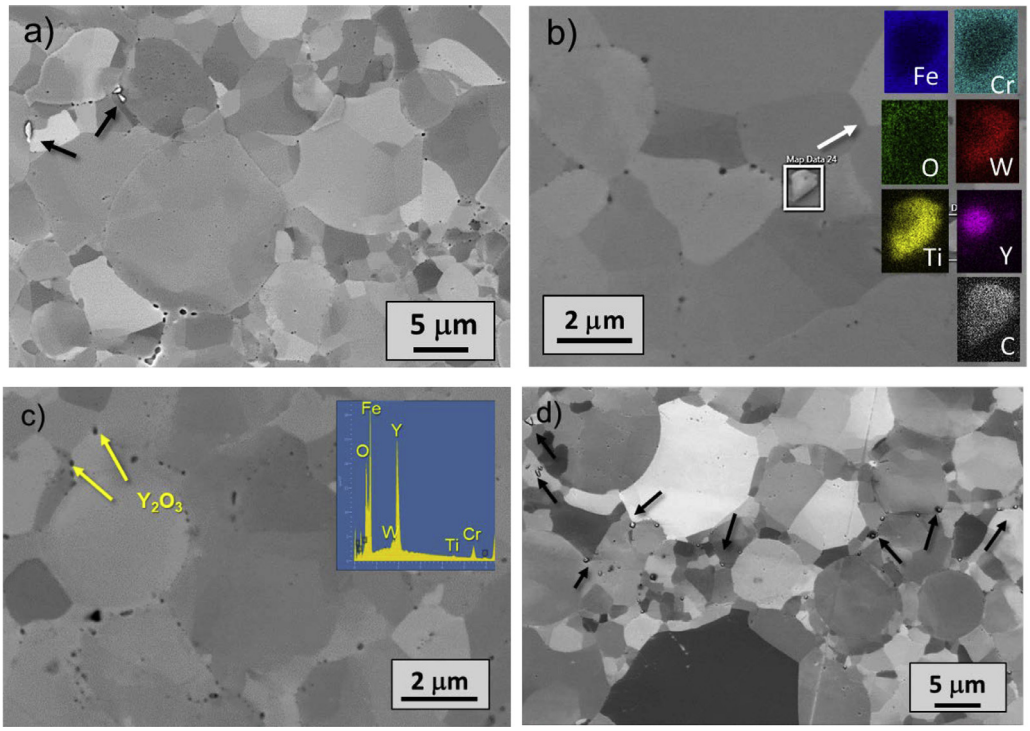

Fig. 4. SEM detailed microstructure of Ceit powders (< 20 μm) consolidated at: (a) and (b) 1220 °C, 2 h, 400 ppm oxygen, (c) 1220 °C, 2 h, 1500 ppm oxygen, (d) 1220 °C, 4 h, 1500 ppm oxygen.

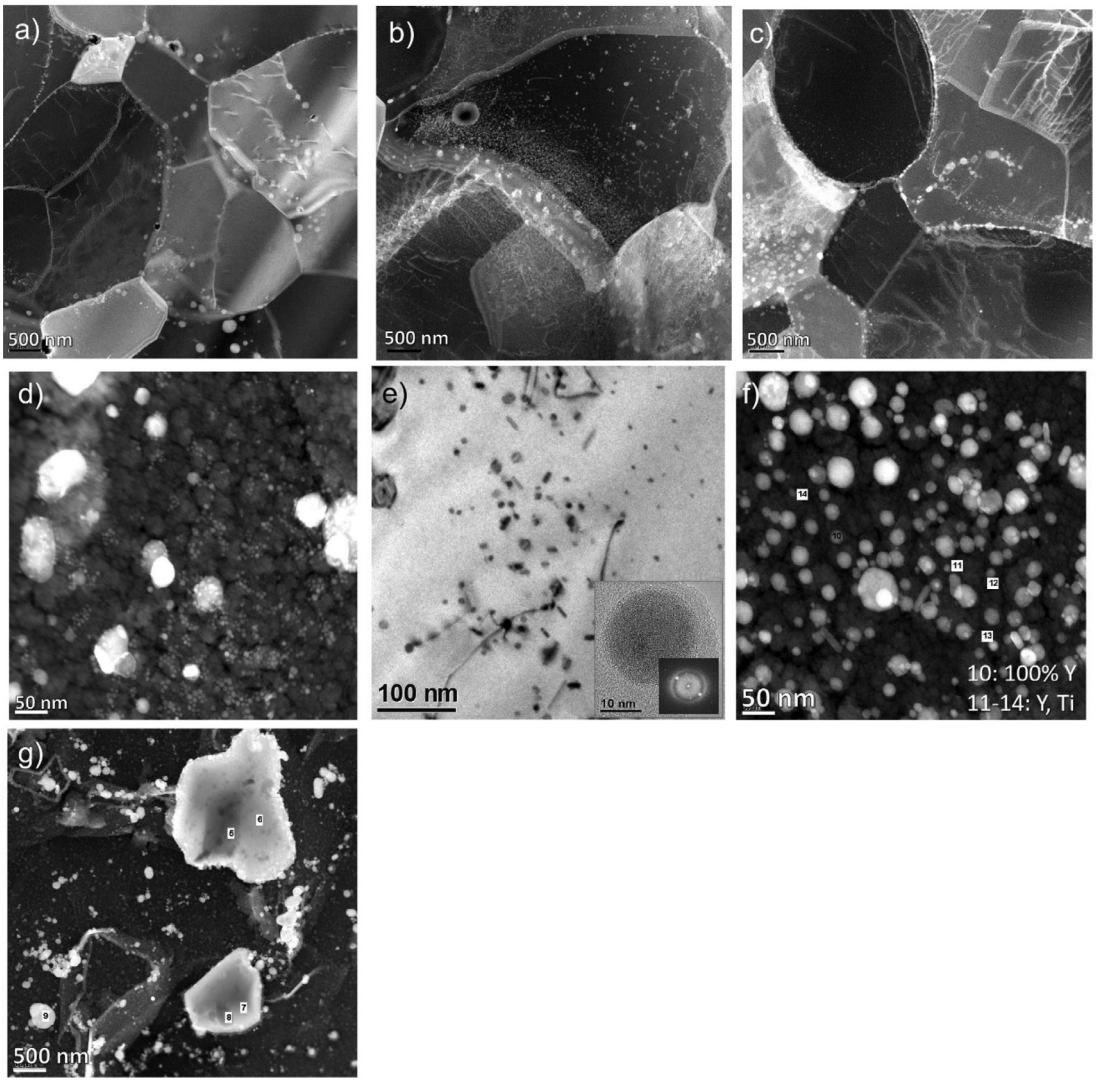

Fig. 5. TEM images after HIP consolidation at: (a) 1220 °C, 2 h, 700 ppm oxygen, (b) 1220 °C, 2 h, 700 ppm oxygen (c) 1220 °C, 4 h, 500 ppm oxygen, (d) 1220 °C, 4 h, 1000 ppm oxygen, (e) 1220 °C, 2 h, 1500 ppm oxygen, (NP identified as bcc-Y_2O_3 in zone axis <132>) (f) 1300 °C, 2 h, 600 ppm oxygen, (g) 1300 °C, 2 h, 300 ppm oxygen. TLS powder: (a), (b), Ceit powder: (c) to (g). Initial powder particle size: (a) to (e) < 20 μm, (f) to (g) 20–45 μm. (a) to (c): STEM images, (e): BF, (d), (f), (g): STEM micrographs of carbon extraction replica.

rich carbides, or in solid solution in the ferritic matrix. Ti- and W-rich particles in samples with a low oxygen concentration were also found by TEM (Fig. 5g). Their atomic Ti/W ratio measured by EDS on carbon replicas was the same as that obtained by EDS in SEM (approximately 9/1).

X-ray absorption spectroscopy results for ODS FS samples and reference compounds (Y_2O_3, Y_2TiO_5, $Y_2Ti_2O_7$, Y foil, Ti foil, TiC) are shown in Fig. 6. The Y K-edge XANES, EXAFS $\chi(k)k^2$ spectra and their Fourier transforms (FTs) of ODS FS samples HIPped at 1220 °C and 140 MPa during 2 h from Ceit powders confirm that yttrium is completely oxidized in the samples with high oxygen content (1500 ppm). However, the results corresponding to the samples with low oxygen content (300–400 ppm) indicate that a significant fraction of yttrium is neither Y_2O_3, $Y_2Ti_2O_7$ nor metallic Y (Fig. 6a–c). This fact, together with EDS analyses performed on several Y-rich large particles (Fig. 4b), suggests incomplete oxidation of yttrium during HIP consolidation of powders with low oxygen concentration. The position of the Ti K-edge XANES of the STARS ODS FS samples agrees with that in metallic titanium (Fig. 6c), suggesting that Ti ions are present in Ceit samples for all oxygen concentrations in the oxidation state close to zero, i.e. in metallic state. Additionally, the fine structure above the Ti K-edge does not correspond to that in the metallic foil. Our simulations suggest that titanium atoms enter ferrite matrix and substitute iron. The results of calculations for titanium located at the iron position in α-iron matrix are shown in Fig. 5d and are in agreement with the experimental data. Minor presence of Ti forming carbides, oxides or intermetallics cannot be excluded completely.

According to Cunnigham [27], the optimum oxygen concentration for an ODS FS with composition Fe-14Cr-0.4Ti-0.2Y, close to that of present work, is 1500 ppm. Since the solid solubility of oxygen in α-Fe is very low (e.g. 0.03 wt.% at 900 °C [26]), the dissociation of PPBs continues provided oxygen diffuses into the grains and reacts with yttrium, until all Y has been consumed. The gradient in the density of NPs with distance to PPBs, observed in all samples (Fig. 5b), despite these PPBs being dissociated and regardless of the oxidation degree, indicates that the actual optimum oxygen uptake of atomized powders has not

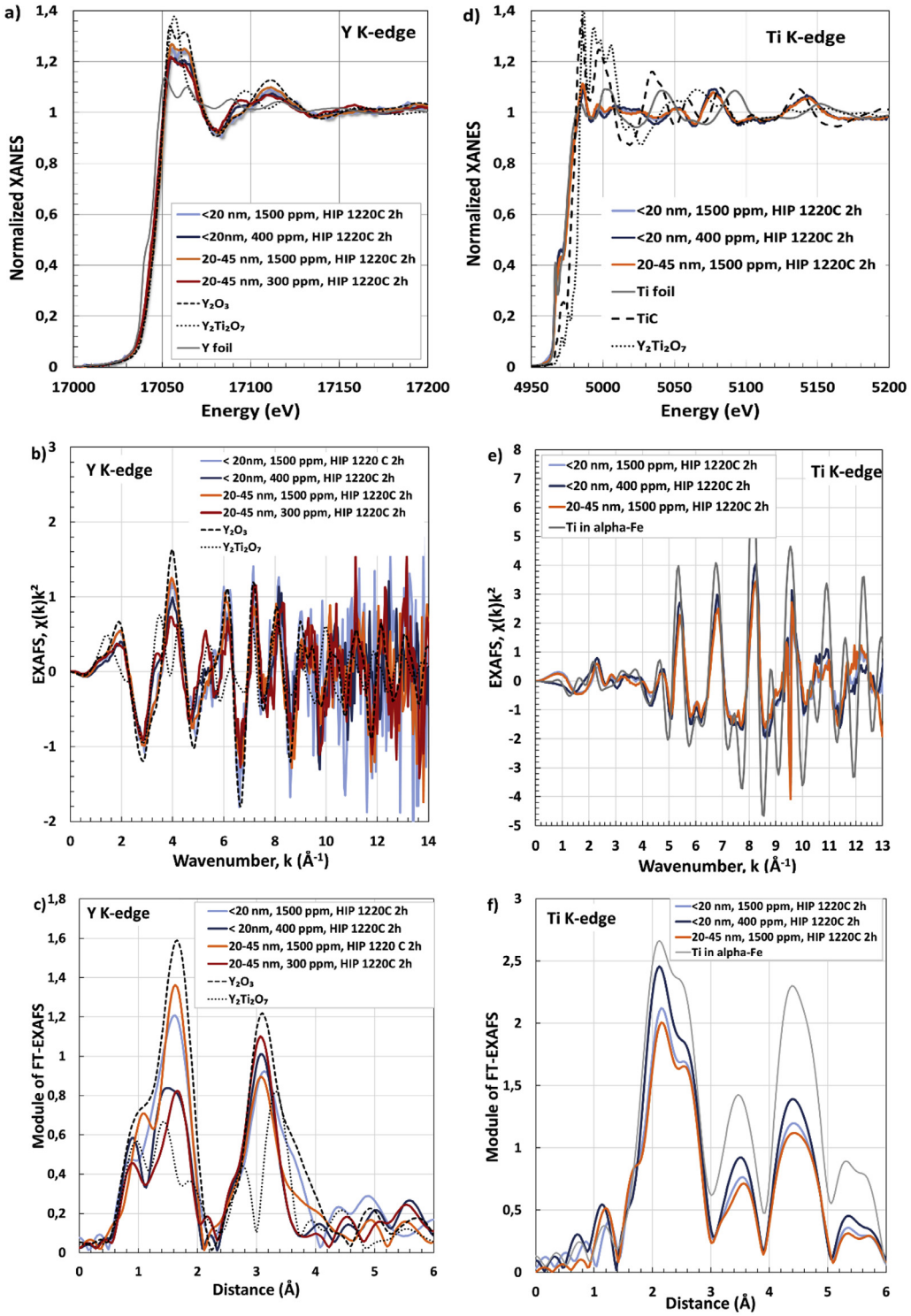

Fig. 6. Y (a–c) and Ti (d–f) K-edge XANES, EXAFS $\chi(k)k^2$ spectra and their Fourier transforms (FTs) of the ODS FS and reference (Y_2O_3, Y_2TiO_5, $Y_2Ti_2O_7$, Ti foil, TiC) samples.

been achieved, but should be increased above 1500 ppm. Summarising, mild oxidation of powders (<1000 ppm) fails in oxidising Y completely, and promotes presence of (Ti,W)C submicrometric particles. Oxidation up to 1500 ppm of oxygen succeeds in preventing (Ti,W)C precipitation, but density of NPs is lower than required (10^{23} m^{-3}) to provide the enhanced strengthening effect, as shown below.

The mechanical strength after HIP at high temperature was low (Fig. 7), due to the low density of NPs, and the presence of large particles. Surface fracture analyses, not shown here, indicated void formation along PPBs, associated to largest Y-rich oxide NPs, and fracture of brittle (Ti,W)C particles, which undoubtedly caused premature failure. The GARS route lead to ODS FS with higher values of yield

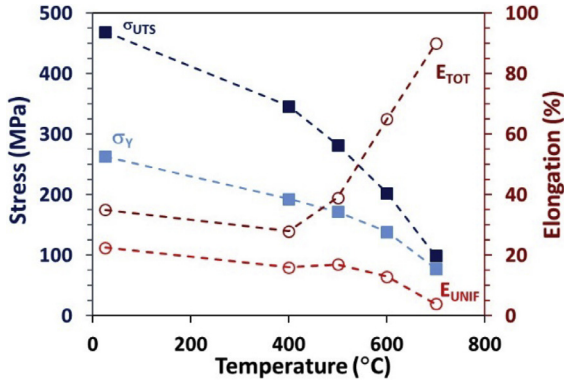

Fig. 7. Mechanical properties of TLS powder (700 ppm oxygen), HIPped at 1220 °C and 140 MPa during 2 h.

strength (~ 400, 350 and 150 MPa at RT, 400 °C and 600 °C, respectively) and ultimate tensile (~ 540, 400 and 150 MPa at RT, 400 °C and 600 °C, respectively) thanks to the cold rolling to an ~80% reduction in area, performed after consolidation [23]. The oxygen concentration has little effect on the hardness: typical values are 150–160 HV1 for 300 < O < 700 ppm, and 160–180 HV1 for 1000 < O < 1500 ppm. The mechanical strength and the hardness of the STARS ODS FS are also lower than the corresponding values of conventional ODS FS [2,6,14,28–30], although comparison is not straightforward because the results presented here correspond to STARS ODS FS before TMTs.

3.2.1. Low temperature consolidation and thermo-mechanical treatment (TMT)

In order to increase the density of NPs, by enhancing the presence of nucleation sites, hot deformation was included as an additional intermediate step in the STARS route. After HIP consolidation at low temperature (900 °C, 140 MPa, 2 h), samples were almost completely dense, and a large fraction of the metastable oxides grown at the surface during oxidation of powder, remained at PPBS. Then, hot deformation, $\varepsilon = 1.1$, performed at 900 °C in a dilatometer equipped with a deformation module, followed by a heat treatment at high temperature (1220 °C, 2 h) promoted oxygen exchange between PPBs and Y and Ti, and a finer and more homogeneous precipitation (Fig. 8), compared to samples consolidated at high temperatures. Also hardness is slightly higher (< 20 μm: 209 HV1, 20–45 μm: 198 HV1).

The kinetics of Y-Ti-O NPs precipitation in the STARS route is controlled by the concentration and the diffusivity of the oxide-forming elements, and the presence of nucleation sites:

- When the temperature is high enough to ensure the dissociation of metastable oxides formed during oxidation of powder, oxygen diffuses from PPBs towards the ferritic grains.
- If the oxygen content available in the ferritic matrix is high enough and the consolidation or heat treatment parameters are adequate, the supersaturated solution of Ti and Y segregate from the ferritic matrix and precipitate to form Y-Ti-O NPs. But, if the oxygen content is below a certain threshold or HIP parameters are severe, Ti- and W-rich submicrometric non-oxide particles (probably carbides) precipitate at GBs. The minimum amount of oxygen to prevent Ti- and W-rich particles precipitation and ensure the complete oxidation of oversaturated Ti is not constant and depends on the HIP parameters, although it is estimated to be above 1000–1500 ppm.
- The inclusion of TMT as an additional intermediate step in the STARS route increases significantly the density of dislocations, which are preferential nucleation sites of Y-Ti-O NPs. As a result, the density of NPs and their distribution in the ferritic matrix is improved.

Detailed investigation to exploit the TMTs as tools to enhance the precipitation of Y-Ti-O NPs is underway.

4. Conclusions

This work confirms that it is possible to achieve a fine control of Ti and Y during atomization following the STARS route at laboratory and industrial scale atomizers. The mechanisms involved in the development of Y-Ti-O NPs in industrial powders are the same as those previously observed in powders atomized at laboratory scale and, therefore, the feasibility of this route at industrial scale has been demonstrated.

The oxygen concentration in the atomized powders and the HIP parameters has a strong effect on the nature and the distribution of NPs. Higher oxidation degree of powders seems to promote the oxidation of Ti and presence of Y-Ti-O NPs, whereas HIPping at highest temperatures and/or long times enhance the precipitation of large Ti- and W-rich particles. In order to increase the density of NPs and achieve complete oxidation of titanium, it is necessary to increase the oxygen uptake after atomization.

The application of hot deformation after HIP at low temperature can be a promising tool in order to improve the distribution of NPs, thanks to the generation of preferential sites (high density of dislocations) for their precipitation, analogously to MA.

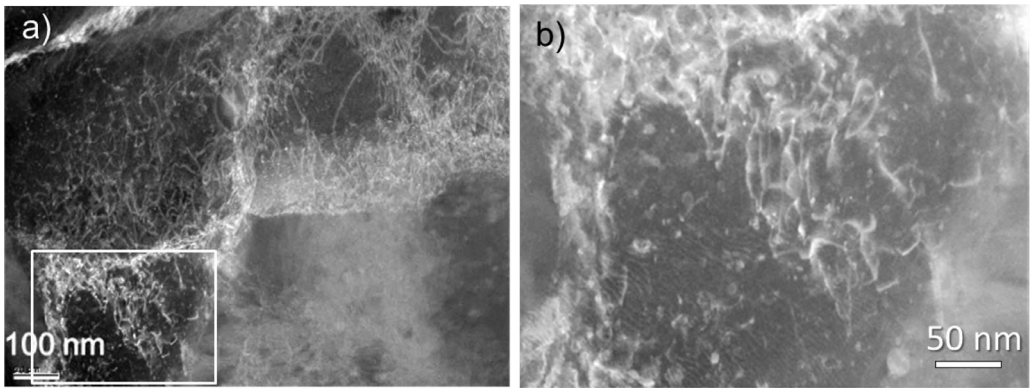

Fig. 8. STEM images of sample consolidated at 900 °C, 2 h, followed by compression at 800 °C and heat treatment at 1220 °C, 2 h. Ceit powder, < 20 μm, 1500 ppm.

Acknowledgements

Authors acknowledge ALBA synchrotron (Spain) for the provision of beamtime on the beam line BL22-CLAESS (Proposal 2016081797). Transmission electron microscopy observations were accomplished at Centro Nacional de Microscopía Electrónica, CNME-UCM. This work has been carried out within the framework of the EUROfusion Consortium and has received funding from the Euratom research and training programme 2014–2018 under grant agreement No 633053. The views and opinions expressed herein do not necessarily reflect those of the European Commission. Financial support from Basque Government through the ELKARTEK ACTIMAT 2016 project is also acknowledged.

Supplementary materials

Supplementary material associated with this article can be found, in the online version, at doi:10.1016/j.nme.2018.06.014.

References

[1] D.T. Hoelzer, et al., J. Nucl. Mater. 367–370 (2007) 166–172.
[2] N. Baluc, et al., J. Nucl. Mater. 417 (2011) 149–153.
[3] G.R. Odette, J. Miner. Metals Mater. Soc. 66 (2014) 2427–2441.
[4] S.J. Zinkle, et al., Nucl. Fusion 57 (2017) 092005–092021.
[5] G.R. Odette, Scr. Mater. 143 (2018) 142–148.
[6] Z. Oksiuta, et al., Mech. Mater. 67 (2013) 15–24.
[7] Y. Sawazaki, et al., J. Nucl. Mater. 442 (2013) S169–S172.
[8] J.P. Wharry, et al., J. Nucl. Mater. 486 (2017) 11–20.
[9] E. Aydogan, et al., J. Nucl. Mater. 486 (2017) 86–95.
[10] C. Suryanarayana, Prog. Mater Sci. 46 (2001) 1–184.
[11] P. Olier, et al., J. Nucl. Mater. 428 (2012) 40–46.
[12] M.K. Miller, et al., J. Nucl. Mater. 351 (2006) 261–268.
[13] P. He, et al., J. Nucl. Mater. 428 (2012) 131–138.
[14] D.T. Hoelzer, et al., J. Nucl. Mater. 471 (2016) 251–265.
[15] G.R. Romanoski, et al., J. Nucl. Mater. 283–287 (2000) 642–646.
[16] M. Klimiankou, et al., J. Nucl. Mater. 367–370 (2007) 173–178.
[17] H. Xu, et al., J. Alloys Compd. 693 (2017) 177–187.
[18] P. Olier, et al., J. Nucl. Mater. 442 (2013) S106–S111.
[19] E. Gil, et al., Fusion Eng. Des. 98–99 (2015) 1973–1977.
[20] E. Gil, et al., Powder Metall. 59 (2016) 359–369.
[21] E. Gil, et al., Appl. Surf. Sci. 427 (2018) 182–191.
[22] N. Ordas, et al., J. Nucl. Mater. 504 (2018) 8–22.
[23] J.R. Rieken., Ph.D. Thesis, Iowa State University (2011).
[24] J.R. Rieken, et al., J. Nucl. Mater. 428 (2012) 65–75.
[25] M.C. Brandes, et al., J. Mater. Sci. 47 (2012) 3913–3923.
[26] J.H. Kim, et al., J. Nucl. Mater. 442 (2013) 458–462.
[27] A. Kuzmin, Physica B 208–209 (1995) 175–176.
[28] R.L. Klueh, et al., J. Nucl. Mater. 314 (2005) 103–114.
[29] J. Hoffmann, et al., J. Nucl. Mater. 442 (2013) 444–448.
[30] M. Dadé, et al., Acta Mater. 127 (2017) 165–177.